Year-long measurements of flow through the Dover Strait by H.F. Radar and acoustic Doppler current profilers (ADCP)

David PRANDLE

Proudman Oceanographic Laboratory, Bidston Observatory, Birkenhead, L43 7RA, UK.

ABSTRACT

Contaminants from the Channel flow through the Dover Strait into the North Sea where they represent a significant fraction of the enhanced concentrations observed along the continental coast. Despite numerous previous investigations, the magnitude of this net flow and its dependency on various forcing factors remain uncertain. The new UK H.F. Radar system, OSCR (Ocean Surface Current Radar) developed for measuring nearshore surface currents offers a clear opportunity of establishing the magnitude and nature of this flow.

Starting in July 1990, H.F. Radar observations were made in the Dover Strait for five months from the French coast overlapping (for two months) with five months from the English coast. These measurements involved fully-automised monitoring of surface currents at 700 locations every 20 minutes. A bottom-mounted ADCP was moored continuously for the same period in the middle of the Strait.

Tidal current atlases were produced from the radar measurements showing ellipses for seven major constituents at up to 160 locations in the strait, examples for the two major constituents M_2 and S_2, are shown in Figures 2 and 3. A net tidal (M_2) residual flow of 36,000 m^3 s^{-1} into the North Sea was calculated from a combination of the M_2 tidal ellipse data with the M_2 tidal elevation distribution.

The localised response of surface currents to wind forcing is shown to follow the classical pattern of Ekman veering, with angles of up to 45° to the wind direction in deep water. In addition to this localised surface response, wind-forced residual currents, persistent through depth and coherent spatially, flow through the strait amounting, on average, to 45,000 m^3 s^{-1}. In addition a steady (non-tidal, non wind-driven) component was observed of approximately 6000 m^3 s^{-1}. Thus net long-term flow into the North Sea was estimated as 87,000 m^3 s^{-1}. i.e. 40 % of earliest estimates and 60 % of the value assumed in many present-day North-Sea models.

The time-averaged residual currents revealed a gyre of approximately 20 km diameter off the westerly edge of Cap Gris Nez rotating anticlockwise with a period of approximately seven days.

These residual flow time-series obtained from the radar measurements are correlated against corresponding time-series obtained from: a) wind measurements; b) the bottom-mounted ADCP; c) flows through the Dover Strait computed by the UK numerical model used operationally to predict storm surges. Significant correlations are found in all cases with a maximum value of 0.8, between the depth-averaged ADCP residual current and the flow through the Strait calculated by the model. These correlations indicate that the low-frequency flows through the Dover Strait determined from the radar measurements on the French and English coasts are generally in opposing directions. Additional preliminary comparisons with observed sea-surface slopes were restricted by the availability of tide gauge data.

Oceanologica Acta, 1993. **16**, 5-6, 457-468.

RÉSUMÉ

Flux dans le Pas-de-Calais mesuré par radar HF et courantométrie acoustique Doppler

Les polluants de la Manche s'écoulent dans le Pas-de-Calais en direction de la Mer du Nord, où ils contribuent de manière significative à l'augmentation des concentrations observée le long de la côte continentale. L'intensité de ce flux et sa relation avec divers facteurs de forçage restent incertaines malgré le nombre des travaux antérieurs. Le nouveau système radar HF du Royaume-Uni, OSCR (Ocean Surface Current Radar), mis au point pour mesurer les courants côtiers superficiels, permet de déterminer l'intensité et la nature de ce flux.

Les observations par radar HF dans le Pas-de-Calais ont commencé en juillet 1990 à partir de la côte française pendant cinq mois, et à partir de la côte anglaise pendant cinq mois, les deux périodes se chevauchant sur deux mois. Une surveillance entièrement automatisée des courantomètres de surface a été effectuée en 700 stations toutes les vingt minutes. Pendant la même période et en continu, un courantomètre acoustique Doppler (ADCP) était ancré sur le fond au milieu du détroit.

Des atlas de courants de marée ont été établis à partir des mesures radar ; ils présentent, pour 160 stations du détroit, les ellipses de sept composantes principales, par exemple M_2 et S_2 sur les figures 2 et 3. L'onde de marée M_2 fait entrer dans la Mer du Nord un flux résiduel net de 36000 $m^3 s^{-1}$, valeur calculée à partir d'une combinaison de données de l'ellipse de l'onde M_2 et de la répartition de la hauteur de l'onde M_2.

La réponse locale des courants de surface au forçage du vent suit le schéma classique de la spirale d'Ekman avec, en profondeur, des courants orientés à 45° de la direction du vent. Outre cette réponse superficielle locale, les courants résiduels forcés par le vent, permanents jusqu'au fond et cohérents dans l'espace, correspondent à un flux dans le Pas-de-Calais de l'ordre de 456000 $m^3 s^{-1}$. Enfin une composante constante (qui n'est due ni à la marée, ni au vent) a été observée, de l'ordre de 6000 $m^3 s^{-1}$. Ainsi le flux net à long terme entrant dans la Mer du Nord est estimé à 87000 $m^3 s^{-1}$, soit 40 % des estimations antérieures et 60 % de la valeur admise dans de nombreux modèles actuels de la Mer du Nord.

Les moyennes temporelles des courants résiduels révèlent un tourbillon d'environ 20 km de diamètre au large de la bordure occidentale du cap Gris-Nez, tournant dans le sens inverse des aiguilles d'une montre avec une période d'environ sept jours. Les séries temporelles sur le flux résiduel obtenues à partir des mesures radar sont corrélées aux séries temporelles correspondantes obtenues à partir : a) des mesures du vent ; b) de l' ADCP ancré sur le fond ; c) des flux dans le Pas-de-Calais calculés à l'aide du modèle numérique du Royaume-Uni utilisé pour prévoir les ondes de tempête. Les corrélations sont significatives dans tous les cas, avec une valeur maximale de 0,8 entre le courant résiduel ADCP moyenné sur la profondeur et le flux dans le Pas-de-Calais calculé par le modèle. Ces corrélations indiquent que les flux à basse fréquence dans le Pas-de-Calais, tels que déterminés par les mesures radar sur les côtes française et anglaise, ont généralement des directions opposées. D'autres comparaisons préliminaires avec les pentes observées de la surface de l'eau ont été limitées par les données disponibles de hauteur de marée.

INTRODUCTION

The Strait of Dover connects the southern North Sea with the English Channel (Fig. 1). These regions are characterised by strong tidal forcing and both are subject to occasional high storm activity. The narrowest section is about 34 km wide with depths of up to 60 m.

The flow of water through the Dover Straits into the North Sea increases the flushing rate of coastal areas along the Continental coast but also transports contaminants originating from both the English Channel and the adjacent Atlantic. For some contaminants this source may be of the order of 50 % of the observed concentrations in this coastal zone. Efforts to determine the long-term rate of this flow and
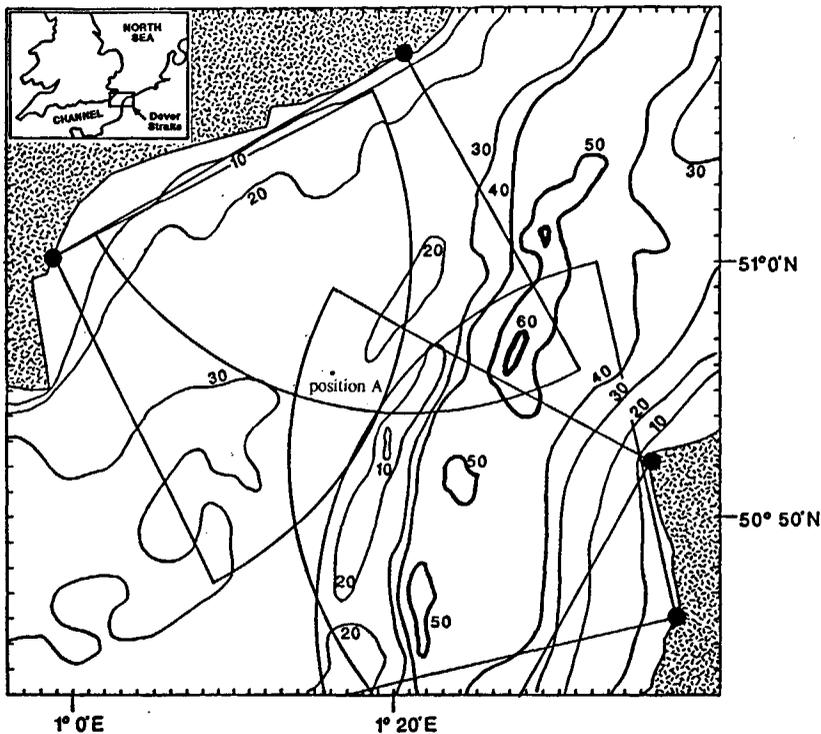
Figure 1

a) Straits of Dover, • radar sites; b) depth contours in metres below chart datum • location of current meter observations (position A).

OBSERVATIONS

H.F. Radar

This study involved up to 6 million current measurements each month (2 dual radar systems x 700 cells x 30 days x 24 hours x 3). The results shown here refer to radar measurements made between June and December 1990 from Cap Gris Nez and Wimereux and between September 1990 and March 1991 from Dover and St. Mary's Bay (Fig. 1). For tidal analysis purposes the data were grouped into monthly sets, five months of data were obtained from both the French and English sites. Table 1 lists the periods over which each monthly set extends.

ADCP

Eleven successful deployments of the bottom-mounted ADCP (developed by the Proudman Oceanographic Laboratory) were completed, with an average data length of thirty days. Consideration here is limited to the five deployments (Tab. 1) that coincided with the radar measurements. The first bin of the ADCP is at a height 3.9 m above the bed and the bin length is 1.4 m. Knight *et al.* (1992) describe these measurements in detail.

its variability with wind-forcing have been made for over sixty years with no definitive value established. The development of the H.F. Radar system, OSCR, by Marex UK promised for the first time, continuous direct observations of surface currents throughout the Strait with sufficient accuracy over a long-enough period to determine this flow (*see* Prandle, 1991 for a review of the principles, performance and applications of the OSCR system).

Simultaneous deployment of a bottom-mounted ADCP provided vertical resolution of the observed currents (at one location). Since contaminants are transported through the straits in both dissolved and particulate form, complementary studies of the latter phase were made concurrently within the EEC *MAST Fluxmanche* programme. This paper considers only the water transport.

Specific objectives were:

1) to measure the net residual flow through the Dover Strait for up to one year;

2) to relate components of this flow to their forcing factors and thereby enable predictions to be made of the residual flow at other times.

The second section outlines the new observational data obtained from the H.F. Radar and the ADCP.

The third section summarises the results from analysis of the tidal components of the radar data while the fourth section summarises corresponding results for the residual components. Fuller details of these results have been described in Prandle *et al.* (1993) and Prandle and Player (1993). The two last sections present intercomparisons of these radar data with results from the ADCP, observed winds and a shelf-wide numerical model.

Table 1

Measurements.

H.F. Radar:	Currents at twenty minute intervals at up to 700 locations Data segmented into thirty day blocks, starting:
English Section:	2 October 1990, 1 November 1990, 1 December 1990, 31 December 1990, 30 January 1991. (all wind data from Langdon)
French Section:	4 July 1990, 18 July 1990, 17 August 1990, 16 September 1990, 23 October 1990. (wind data for months 1 and 2 from both Lydd and Langdon, months 3 Lydd and months 4 and 5 Langdon)
ADCP data:	Currents measured at ten minute intervals Data analysed from bins at 3.9, 5.3, 6.7 and 8.1 m above the bed, total depth = 30 m .
Deployments:	18 July-21 August 1990, 4-24 September 24 September-18 October 1990, 18 October-20 November 1990, 20 November-18 December 1990.
STWS data:	1 September 1990 to 26 March 1991.

Wind data

Wind data were supplied from the UK Meteorological Office at hourly intervals from Lydd (50° 56'N, 0° 54'E) and Langdon (51° 7'N, 1° 20'E). Lydd is a low lying site where winds were expected to approximate those over the adjacent sea. Unfortunately, malfunctioning of the anemometer entailed the use of alternate data from Langdon. Table 1 shows the origin of each set.

TIDAL COMPONENTS OF THE RADAR

Tidal ellipse measurements

The elevation amplitude, at Dover, of the predominant constituent M_2 is 2.23 m followed by S_2 with an amplitude of 0.71 m and N_2 with amplitude 0.41 m. Prandle (1980) produced co-tidal charts for the southern North Sea and Straits of Dover region for these three major constituents together with the diurnal constituents O_1 and K_1 and the higher harmonics M_4 and MS_4.

The pre-determined cell configurations for the OSCR measurements generally consisted of a rectangular 1km spacing over the first 20 km range and 2 km beyond. With present interest in broader scale features, vector averages were calculated for all ellipses within rectangular regions 1' of latitude and 2' of longitude (*i.e.* 2.5 km squares). Thus with an OSCR cell spacing of 1km each ellipse represents an average of six values. This geographic synthesis was then used as a data quality check requiring that within each square, the standard deviation of current amplitude σ_A and phase σ_P and direction σ_D were within prescribed limits (4 cm s⁻¹ for

σ_A and 4° for both σ_P and σ_D for the predominant semi-diurnal constituents).

This geographic synthesis was then extended temporally, combining results for successive months from each region subject to similar checks on consistency. Thus, the final values shown represent an average from typically thirty separate analyses. Figures 2 and 3 show tidal ellipses obtained for the M_2 and S_2 constituent.

Prandle *et al.* (1993) show similar distributions for a further five constituents together with detailed comparisons of these new observational results against values obtained from a numerical model.

The smooth even sweep of the M_2 tidal currents through the straits is typical of distributions measured elsewhere with OSCR. The eccentricities are generally less than 0.1 with clockwise rotation in all but 20 (in the S-E corner) of the 159 ellipses shown. The amplitudes vary widely from a maximum of 143 cm s⁻¹ immediately off Cap Gris Nez to less than 40 cm s⁻¹ at the western edge. These amplitudes are in broad agreement with earlier current meter measurements. The surface tidal currents tend to align with the large scale topographic features through the straits and do not adjust to the sharply varying local topography.

The phases shown in Figure 2 indicate advances to the west and near the French coast [phase advances in shallower water near coastal boundaries can be related to the influence of bed-friction Prandle (1982)].

The S_2 tidal current ellipses (Fig. 3) exhibit the same smooth sweep as for M_2 with similarly good agreement with current meter recordings. The amplitude of the OSCR ellipses range from 14 to 44 cm s⁻¹ the latter value corresponding in location to the maximum M_2 value of 143 cm s⁻¹. The ratio of these S_2:M_2 maxima, 0.31, agrees closely with the ratio of elevation amplitudes at Dover.
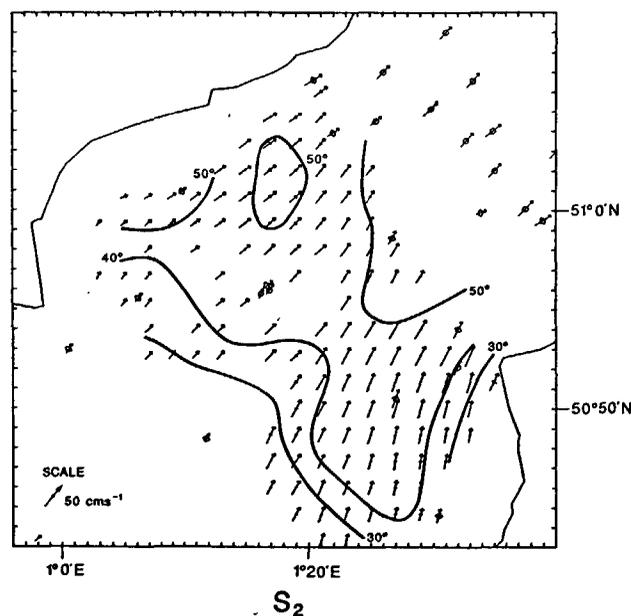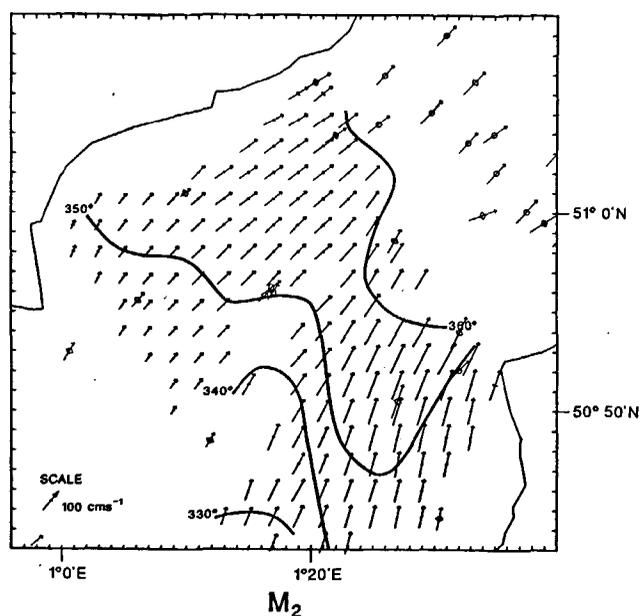
Figures 2-3

Tidal Current Ellipses (2) M2, (3) S2. Longer line represents magnitude of the semi-major axis, shorter line the semi-minor axis. Values shown are from monthly analysis of OSCR measurements with vector means over: a) adjacent 2.5 km rectangle; and b) five months of data on the French side and five months from the English. Superposed are corresponding data from Admiralty tidal diamonds and current meter moorings (labelled with a small circle).
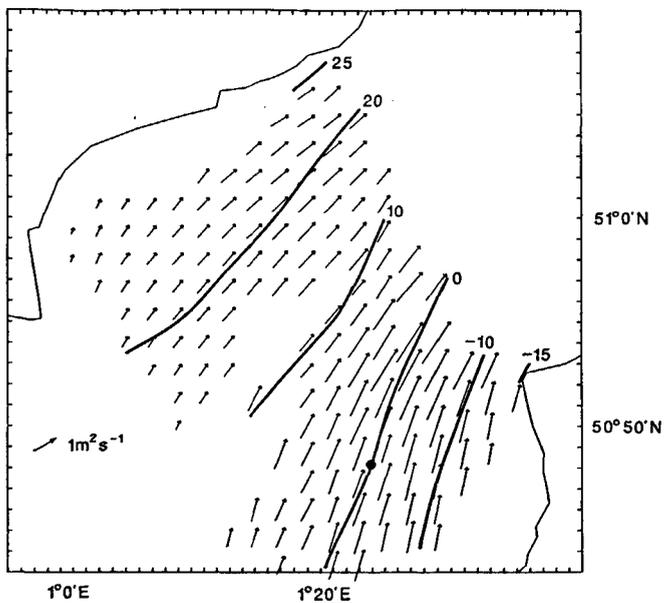
Figure 4

Residual flows associated with M_2 tidal propagation. Streamline units 1000 $m^3 s^{-1}$, •, $\psi = 0$ (arbitrarily designated).

M_2 residual flux

The net residual flow, S_T, over a tidal cycle associated with the M_2 tidal current ($\hat{U}$, θ) (confined to one direction) and elevation (ζ, g) in water depth D is

$$S_T = \frac{1}{P} \int_0^P \hat{U}\cos(\omega t - \theta) [D + \zeta\cos(\omega t - g)] \, dt$$

$$= \frac{1}{2}\hat{U}\zeta\cos(\theta - g) \tag{1}$$

Substituting ($\hat{U}$, θ) from the semi-major axis of the OSCR tidal ellipse data (Fig. 2), the residual flows were, on average, 10 % greater than calculated using a vertical current structure model (based on the linearised vertical structure equation 9 with a constant eddy viscosity coefficient) and the residual directions from the model were, on average, only 1° (anticlockwise) different from that of the ellipse axis.

Calculations were also made of the influence of M_4 and M_6 constituents of both $\hat{U}$ and ζ on the residual fluxes, in this application these were shown to contribute less than 1 % to net fluxes. Thus here we make calculations of tidal residual flow based solely on the observed M_2 surface currents measured by OSCR (with ζ and D). These fluxes should reasonably approximate the averaged values resulting from all tidal constituents.

The residual streamline ψ distribution corresponding to these point-values of depth-averaged residual flows were constructed using a harmonic smoothing function to best fit the relationships

$$\frac{\partial\psi}{\partial y} = D\overline{U}_0 \text{ and } \frac{\partial\psi}{\partial x} = -D\overline{V}_0 \tag{2}$$

where $(D\overline{U}_0, D\overline{V}_0) = S_T$.

This functional representation of ψ accounted for approximately 75 % of the variance along both the x and y axes. Figure 4 shows the resulting distributions together with the point values of (DU_0, DV_0), and the arbitrary zero reference point for ψ. This component of net residual flow through the channel amounts to 40,000 m^3 s^{-1} (or 36,000 m^3s^{-1} based on depth-averaged velocities) with the greater proportion concentrated on the French side.

Model estimates of net residual flow in m^3s^{-1} (associated with M_2 tidal propagation) include: Pingree and Maddock (1977), 5 x 10^4, Pingree and Griffiths (1980), 3 x 10^4, Prandle (1984), 5 x 10^4, POL 35 km shelf model 4.6 x 10^{-4}, POL 9 km shelf model 3.8 x 10^4. The 36,000 m^3 s^{-1} value from this radar study is shown to be closest to that of the POL 9 km shelf model.
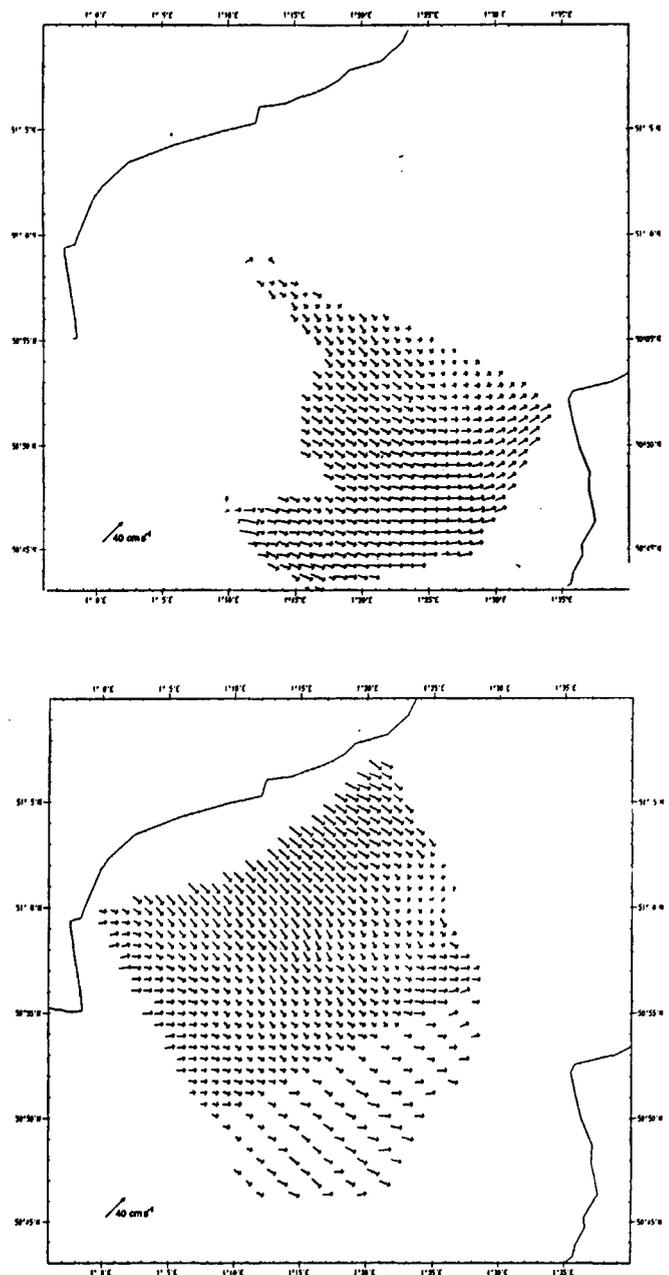
Figure 5

Surface current response to wind of 10 m s^{-1} from the west. a) French section; b) English section.

RESIDUAL COMPONENTS OF THE RADAR MEASUREMENTS

The wind-driven component is first studied by correlation, at each position, of the residual surface currents against locally observed winds. Larger scale organised motions are then examined using modal analysis with the time-series pertaining to these modes subsequently correlated against wind data. The horizontal circulations of the monthly-averaged remaining (non-tidal, non-wind driven) residual currents are then examined.

Localised response

The following "open-sea" relationship between the residual surface current vector (at each position) R(t) and wind vector W(t) was assumed for any time (t).

$$R(t) = R_0 + \alpha W(t - \delta t) |W(t - \delta t)| \qquad (3)$$

where R_0 is a constant residual current independent of wind forcing, α is a vector coefficient relating the amplitude and veering of the wind driven current relative to the wind direction and δt is a time lag.

A least squares fitting procedure was used to derive R_0 and α for a range of values of δt. Figure 5 shows typical values of α from both the French and English section. The overall mean value of α is 16 cm s^{-1} for a 10 m s^{-1} wind with mean veering 20° clockwise. Figure 8 shows corresponding values of the constant residual current R_0.

Assuming the expression for surface wind-driven currents R_W given by Prandle and Matthews (1990)

$$R_W = -\frac{\tau_w i^{1/2}}{\rho(fE)^{1/2}}\left(1 + \frac{Eb - K}{K \exp(bD)}\right) \qquad (4)$$

the results shown are consistent with a value of E $\propto$ 0.005 m^2 s^{-1} for $\tau_w = \rho$ 0.0013 W^2 N m^{-2}.

Large-scale response

Modal analysis

Modal analysis is well-suited for identifying organised motions within vector time series recorded at a number of locations, in particular rotary "empirical orthogonal function" (EOF) analysis has been widely used for ocean currents (Klinck, 1985; Prandle, 1987). To minimise gaps in the time-series for modal analysis hourly averages were calculated from consecutive sets of twenty minute values. These hourly time series from each position were then averaged over all positions within a rectangular 2.5 km grid (vector averages were used both temporally and spatially).

For both sets of data, a predominant mode existed accounting for 40 % of the total variance in the French residual current data and 30% in the English data. These modes are shown in Figure 6 rotated (relative to a nominal easterly direction) by 33° and 11° respectively. These rotations reflect the predominant orientations of their

corresponding (complex) "eigenvalue" time series. These time series include substantial (incoherent) tidal energy, a running tidal filter was used to remove this semi-diurnal (tidal) energy. The filtered time series $M_0(t)$ was calculated by least squares fitting of the expression

$$M_0(t) + at + b \cos\omega t + c \sin\omega t \qquad (5)$$

to values up to six hours before and after the time concerned ($\omega = 2\pi/12.42$ h). The overall effect was to reduce the average variance by 40 % for the French data and 60 % for the English data.

Histograms of the orientation of the "eigenvalue" time series for the French data showed that the orientations were between 22.5° to 45° [or 202.5° to 225° (measured
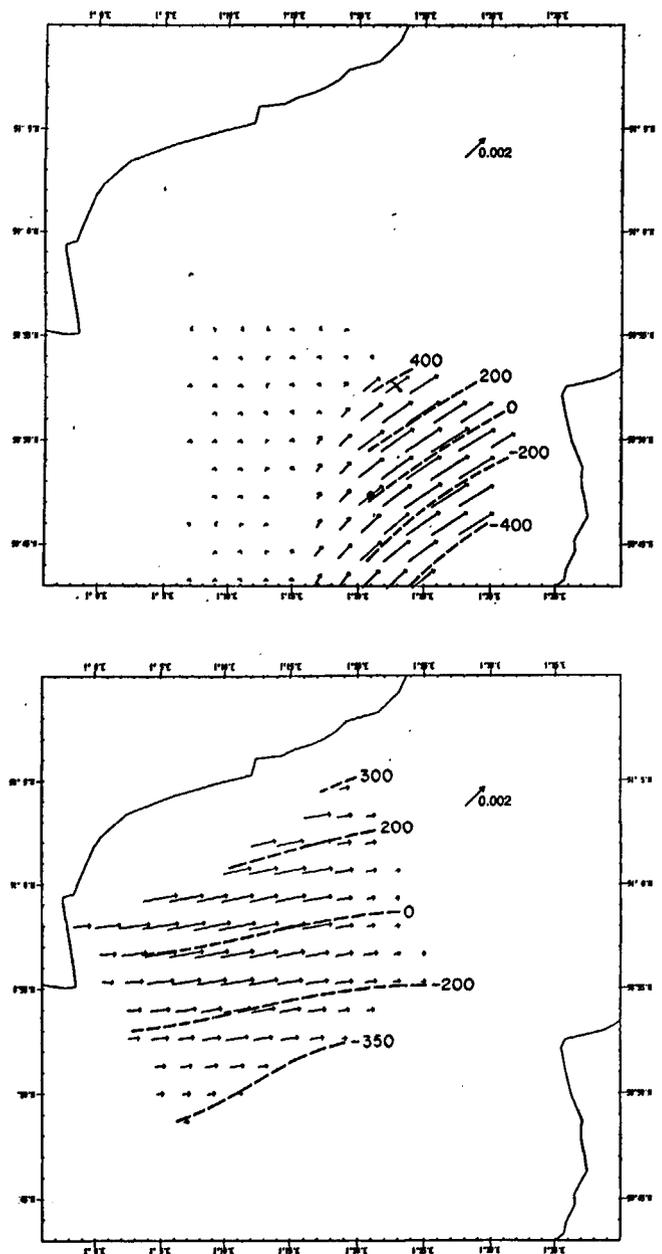
Figure 6

Vectors from first modes of EOF analyses. a) France, rotated 33° a-c from east; b) England, rotated 10° a-c from east. Units: 1) vectors m s^{-1} when multiplied by a unit of the time series shown in Figures 7 a and b; 2)"streamlines" indicate net flows in m^3 s^{-1} when multiplied by a unit of the modal time series Figure 7.
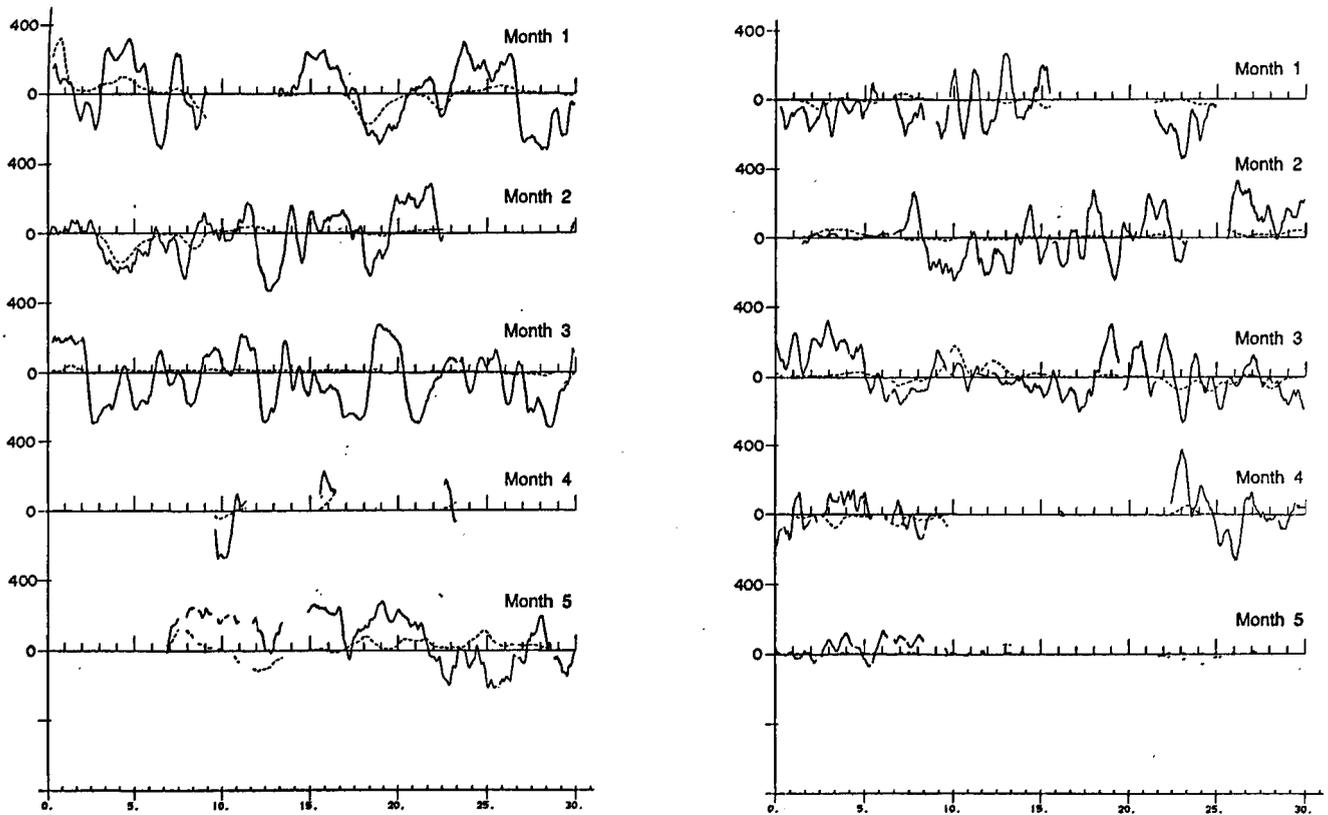
Figure 7

First modal time series resolved along principal axes. a) French data along 33° (a-c from east); b) English data along 11° dashed lines indicate best fits to wind time series (equation 6). Units: m s⁻¹ when multiplied by a unit vector shown in Figure 6.

anti-clockwise from east)] for 67 % of the time (*cf.* 12.5 % for a random distribution) and this time accounted for 88 % of the total amplitude.

Likewise for the English data the orientation was between 0° and 22.5° (or 180° to 202.5°) for 74 % of the time representing 87 % of the total amplitude. Thus to more readily visualise the flow patterns associated with these predominant modes, their vector time series were approximated by components resolved along the principal axes 33° and 11° respectively (Fig. 7 *a* and *b*).

The modal (scalar) time series $M(t)$, resolved along these principal axes, were then related to the east and north components of wind $W(t)$, (W_E and W_N respectively), by the expression,

$$M(t + \Delta t) = M_0 + C_E W_E(t) |W(t)| + C_N W_N(t)|W(t)| \qquad (6)$$

where Δt represents a time lag between the wind forcing and the resulting current.

For the French side a best fit was found for (correlation coefficient $r = 0.318$ for 2348 data points)

$$M_0 = 8.1, C_E = -0.28, C_N = -2.27, \Delta t = -36 \text{ h}$$

while for the English side ($r = 0.239$ for 2458 data points)

$$M_0 = 3.2, C_E = -0.16, C_N = 0.65, \Delta t = 9 \text{ h}$$

The time lags (or advance in the French case) may be related to the time difference between the wind at the selected meteorological sites and the wind over the regions

where these flows are generated. In a later section ("Intercomparison of the H.F. Radar surface current measurements with ADCP measurements, wind observations and numerical simulations"), larger correlation coefficients are found between these radar measurements and comparable flows derived from both a moored ADCP and a shelf-wide numerical model. These relatively small correlations between the radar measurements and the local wind are attributed to: a) forcing of through flow by other than "localised" winds; and b) the complex dynamic response of non-tidal surface currents to the original forcing.

The modal patterns in Figures 6 *a* and 6 *b* can be translated into streamline flows as described below. These streamlines, superposed on the modal currents, indicate net flows of approximately 800 m³ s⁻¹ and 650 m³ s⁻¹ (per unit eigenvalue as per equation 7). The two modes conveniently overlap in mid-channel and represent total flow F_T in $m^3 s^{-3}$ of

$$F_T = (8.1 - 0.28 \ W_E \ |W_E| - 2.27 W_N \ |W_N|)800$$
$$+ (3.2 - 0.16 \ W_E \ |W_E| + 0.65 \ W_N \ |W_N|)650 \qquad (7)$$

The above analyses assume the surface residual currents extend uniformly throughout the depth. A factor $\alpha = R$ surface/R is introduced to correct for this assumption.

In the absence of wind, $F_T = 8\,560 \ \alpha \ m^3 \ s^{-1}$, for an easterly wind $F_T = -328 \ \alpha \ W_E \ |W_E|$ and for a northerly

wind $F_N = -1394 \alpha W_N |W_N|$, the latter two may be combined to yield

$$F_W = 1432 \alpha W^2 \cos(\theta - 77°) = 1432 \alpha W^2_{cos} (\phi + 167°) \quad (8)$$

where θ is the direction towards which the wind blows and is here measured anti-clockwise from east and ϕ is the conventional direction from which the wind blows and measured clockwise from North.

Comparable values are as follows:

Prandle (1978) $F_W = 2400 W^2 \cos(\theta - 60°)$
$= 2400 W^2 \cos(\phi + 150°)$

Prandle (1984) $F_W = 1100 W^2 \cos(\theta - 74°)$
$= 1100 W^2 \cos(\phi + 164°)$

Pingree and Griffiths (1980) $F_W = 1600 W^2 \cos(\theta - 83°)$
$= 1600 W^2 \cos(\phi + 173°)$

Oerlermans (1978) $F_W = 1100 W^2 \cos(\theta - 66°)$
$= 1100 W^2 \cos(\phi + 156°)$

Intercomparison of these results is complicated by differing assumptions regarding: a) the relationship between wind speed and surface stress; and b) the selection of appropriate wind stations.

Later, in the next section, it is shown that at position A, $\alpha = 0.75$, for this value, the present result (8) is within the range of results previously derived.

Oscillatory components

Oscillations in the modal time series, show maximum values up to approximately ± 400 compared with mean values (equation 9) of 8.1 and 3.2 for the French and English data sets respectively. From the earlier streamline calculations, these maxima are equivalent to cross-sectional net oscillatory flows of up to $6 \times 10^5 m^3 s^{-1}$. Their periodicities are typically 20 to 30 hours. In a numerical simulation of the extreme 1953 storm surge, Prandle (1975) estimated maximum flows through the Dover Strait of $2.6 \times 10^6 m^3 s^{-1}$. For the long-term mean wind stress components $\tau_x = 0.04 N m^{-2}$ and $\tau_y = 0.05 N m^{-2}$ estimated by Prandle (1984), (8) indicates a net wind-driven flow of $60 \alpha 10^3 m^3 s^{-1}$.

Steady state residual component

Figures 8 *a* and *b* show typical steady state residual surface currents for a monthly data set after removal of: a) the tidal component; and b) the (localised) wind forced component.

The outstanding feature is clearly the well-defined gyre off the French coast where currents around its extremity exceed 20 cm s^{-1}. The diameter of the gyre exceeds 20 km and it is present in all five monthly data sets, though perturbed by monthly variations in the background flow. The circulation on the English side is less clear, though components of the structure are common to several of the monthly sets.

The mean residual currents averaged over the spatial field of the complete five months of data used for the modal analyses were less than 0.25 cm s^{-1} for both France and England. Thus there is no evidence of a major long-term Eulerian residual flow through the Channel. Likewise the monthly means do not suggest a significant seasonal component (other than that related to wind forcing).

ANALYSIS OF THE RESIDUAL COMPONENT OF ADCP MEASUREMENTS

A simple analytical representation of the vertical structure of wind-driven residual currents is first developed. This theory is then used to examine the ADCP measurements from position A.

The vertical structure of wind-driven residual currents

Omitting time-varying, density gradient and non-linear terms, the horizontal momentum equation simplifies to:

$$g\nabla\zeta + ifR = \frac{\partial}{\partial Z} E \frac{\partial R}{\partial Z} \quad (9)$$
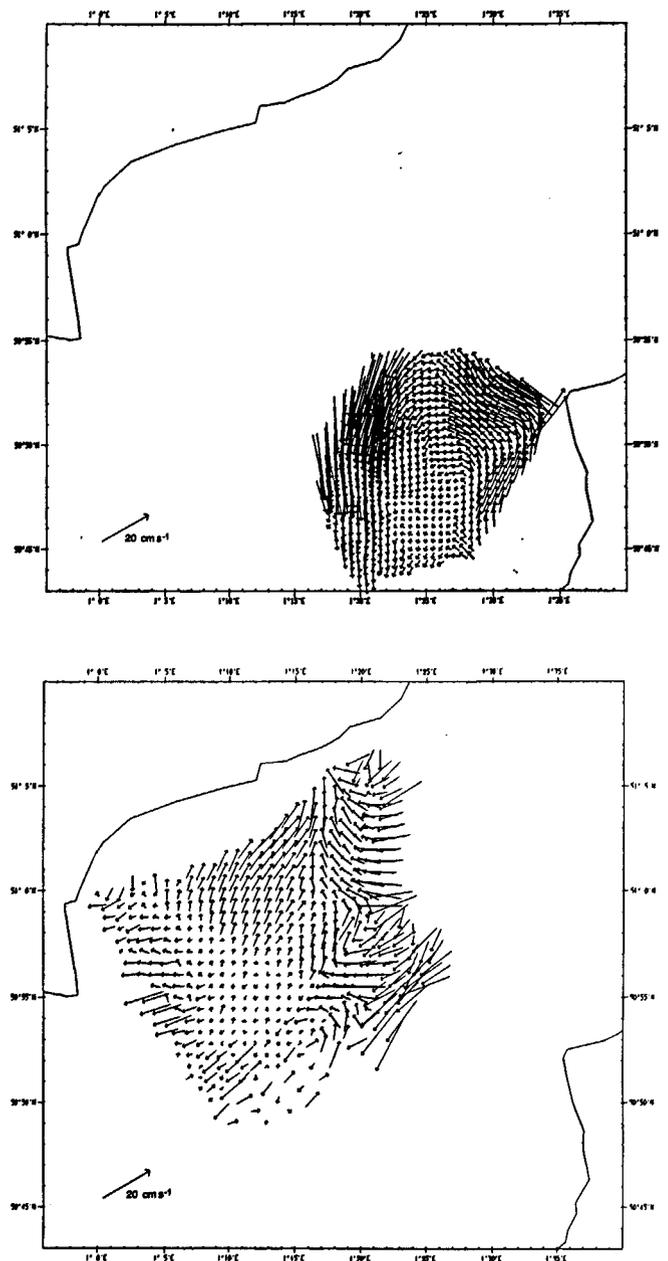
Figure 8

Monthly mean residual currents (tidal and wind-forced components removed). a) French coast; (b) English coast.
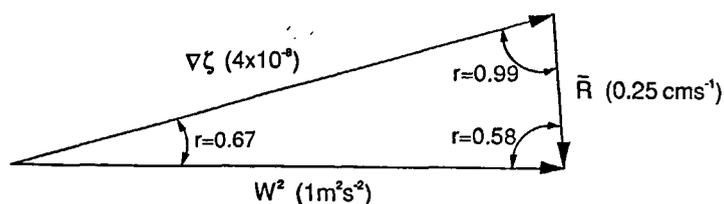
Figure 9

Complex correlations (r, θ) between W^2, $\bar{R}$ and $\nabla\zeta$ for ADCP deployment 20 November 1990 to 18 December 1990. Correlated amplitudes, r, shown; orientations of W^2, $\nabla\zeta$ and $\bar{R}$ represent values of θ. Mean variances shown in brackets.

where R is the velocity at height Z above the bed, g is gravitational acceleration, ζ is the elevation of the sea surface, f the Coriolis parameter and E a vertical eddy viscosity parameter (constant). Neglect of the density gradient term seems justifiable in all but coastal areas of the Dover Strait, however the non-linear terms could contribute additional spatial structure to the results presented here.

Adopting the solution

$$R = A_1 e^{bz} + A_2 E^{-bz} + C \tag{10}$$

requires $b^2 = i\dfrac{f}{E}$ and $C = i\dfrac{g\nabla\zeta}{f}$ (11)

A mean value of E = 0.02 m^2 s^{-1} was calculated by least squares fitting of the vertical profile of observed M_2 tidal current ellipses to the theoretical values of Prandle (1982). This depth-averaged value is four times the "near-surface" value determined for localised wind-driven currents in the "Localised response" section.

At the sea surface, z = H, the wind stress τ_w was taken as

$$\tau_w = 1.3 \times 10^{-3} W^2 \ (N\,m^{-2}) \tag{12}$$

where W is the observed wind speed in m s^{-1}.

From (10) $\tau_w = \rho E \dfrac{\partial R}{\partial Z} z = H = \rho E b (A_1 e^{bH} - A_2 e^{-bH})$ (13)

This equation can be used to relate A_2 to A_1, then (10) can be fitted to the observed vertical profile of residual currents to calculate both A_1 and C. As a test of the resulting profiles, the value of the quadratic bed-stress coefficient K_1 was calculated from

$$\frac{4}{\pi} k |\hat{R}| \bar{R} = E \frac{\partial R}{\partial Z} z = 0 \tag{14}$$

where $|\hat{R}|$ the tidal velocity amplitude ~ 0.5 m s^{-1} and $\bar{R}$ is the residual velocity, the over-bar indicating a depth-averaged value. A complex correlation coefficient (.934, 25°) was calculated for this relationship along with a value of k = 0.0025 *i.e.* the value commonly assumed in 2-D tidal models.

The mean ratio of the depth-averaged value to the residual current at the surface $R_{z=H}$ was found to be close to 0.75 for all 5 ADCP deployments, $R_{z=H}$ is also rotated 5° a-c from $\bar{R}$ on average.

Relationship between $\bar{R}$, $\nabla\zeta$ and W at position A (ADCP mooring position)

The above model was used to compute both the surface gradient $\nabla\zeta$ and the depth-averaged velocity $\bar{R}$ for observed values of W. ADCP current measurements at

heights 3.9, 5.3, 6.7 and 8.1 m above the bed in a total height of 30 m were used in these calculations. Figure 9 shows the relationships derived between $\nabla\zeta$, $\bar{R}$ and W. (these values refer to the deployment 20 November 1990 to 18 December 1990 - similar relationships are computed for all five deployments). The parameters $\bar{R}$ and $\nabla\zeta$ are almost exactly correlated along orthogonal directions. The wind is significantly correlated with both $\bar{R}$ and $\nabla\zeta$ and is more closely aligned with $\nabla\zeta$.

The relationships shown may be compared with the depth-integrated form of (10),

$$g\nabla\zeta + if\bar{R} = \frac{(\tau w/\rho) - (4/\pi)k |\hat{R}| \bar{R}}{H} \tag{15}$$

Substituting g = 9.81 m s^{-2}, f = 0.0001s^{-1}, ρ = 1000 kg m^{-3}, H = 30 m we obtain

$$\frac{\bar{R}}{3.8 \times 10^{-4}} (1,62°) + \frac{\nabla\zeta}{4.4 \times 10^{-9}} = W^2 \tag{16}$$

The relative magnitudes of the terms in equation (16) can be estimated by substituting the values derived from observations in Figure 9 for the case of W = 1 m s^{-1}. The first term, involving $\bar{R}$ has an amplitude of 6.6, the second, involving $\nabla\zeta$, of 9.0 and the third involving W, of 1.0. Thus the values of both $\bar{R}$ and $\nabla\zeta$ are not simply a response to local wind forcing but represent a response to forcing over a much wider area that generates sea surface gradients an order of magnitude greater than calculated locally for $\bar{R} = 0$. However the large correlations computed between $\bar{R}$ and $\nabla\zeta$ with W indicate that this larger area forcing is also correlated with the local wind W. This analysis illustrates why, in the following section, observed and computed flows through the straits are only partially correlated with localised wind forcing.

INTERCOMPARISON OF H.F. RADAR SURFACE CURRENT MEASUREMENTS WITH ADCP MEASUREMENTS, WIND OBSERVATIONS AND NUMERICAL SIMULATIONS

Complex correlation coefficients are calculated between

a) the modal time-series for both the French radar measurements, F, and the English radar measurements, E;

b) the depth-averaged residual currents $\bar{R}$ and surface slopes $\nabla\zeta$ calculated for the ADCP measurements as described above;

c) the observed wind W (strictly W|W| with W measured in the direction towards which the wind blows); and

d) the residual flow through the strait, M, computed by the

POL 35 km 2-D numerical model used for operational storm-surge forecasting (Flather *et al.*, 1991).

Hourly values were used in all cases, the extent of each data set is shown in Table 1. Additional correlations were made against the observed sea-surface slope between Dover and Lowestoft. However this produced low correlations in all cases and hence these values are omitted. It is evident from the previous section that residual values of $\nabla\zeta$ are nearly orthogonal to $\bar{R}$ and hence further consideration of observed sea-surface slopes will be made when tide gauge data are obtained from the French coast and from the Channel section of the English coast.

Table 2 shows these correlations, amplitudes are followed by inclinations where these show the rotation (a-c) of the row parameter relative to the column parameter. Likewise the lags (or advance for a negative lag) represent the delay of the row parameter relative to the column parameter.

The relationships between $\bar{R}$, $\nabla\zeta$ and W have been discussed in the previous section.

The results for correlation with wind W and model M are summarised in Figures 10 and 11 respectively. These

Table 2

Complex correlation coefficients between: *W: wind speed squared*, $\nabla\zeta$ and *R residual surface gradient and depth-averaged current calculated from the ADCP measurements, M, E and F net residual flows through the Dover Strait from a numerical model and English and French radar measurements.*

AMPLITUDES

	W	$\nabla\zeta$	$\bar{R}$	M	E
$\nabla\zeta$	0.44				
$\bar{R}$	0.32	0.95			
M	0.46	0.70	0.80		
E	0.25	0.47	0.45	0.28	
F	0.25	0.31	0.35	0.37	0.27

INCLINATIONS

1					
- 115	- 106				
- 117	- 68	34			
83	101	- 148	180		
- 124	- 74	37	0	180	

NUMBER OF DATA POINTS

3 175					
3 175	3 266				
3 415	1 845	1 845			
2 466	1 424	1 425	1 730		
2 249	1 638	1 638	986	462	

LAGS (HOURS)

- 6					
- 12	0				
- 18	1	1			
- 12	- 3	- 2			
- 36	- 24	- 24	- 18	- 18	

Figure 10

Complex correlations (r, θ) between W^2 and M, E, R, $\bar{R}$ and $\nabla\zeta$. Arrow lengths indicate correlation amplitude r, arrow directions represent - θ i.e a wind blowing towards this direction is most effective in generating M, E and F. Likewise a wind blowing towards this direction generates $\bar{R}$ and $\nabla\zeta$ directed eastwards. Variances corresponding to $W^2 = 1m^2\ s^{-2}$ shown in brackets. W wind speed, $\bar{R}$ depth-averaged residual current and $\nabla\zeta$ residual sea-level gradient calculated from ADCP current profiles. M, E and F flows through the Dover Strait from a numerical model and English and French radar measurements.

figures also show the variance associated with each parameter for a unit value of W(1 m s^{-1}) and M(1 m^3 s^{-1}). The highest correlation with W is against the modelled flow M indicating a maximum new flow for winds aligned along a N-E to S-W axis of

$$F_M = 870\ W^2\ m^3\ s^{-1} \tag{17}$$

Inserting in (8) derived from the radar measurements, the value for the factor $\alpha = 0.75$ (the ratio of $\bar{R}/R_{z=H}$ found earlier), gives $F_W = 1074\ W^2\ m^3\ s^{-1}$, *i.e.* reasonably close to the numerical model result.

Table 2 shows a correlation coefficient between the two radar components, E and F, of r = - 0.27 with F leading E by 18 hours. This result emphasises the opposing components of flow between the French and English sections. The correlations between E and F with $\bar{R}$ indicate that residual currents observed at site A by the ADCP are more closely aligned with the French section (R lagging F by 24 hours), whereas $\bar{R}$ effectively opposes E in direction. The simultaneous existence of residual flows in opposing directions across the strait was first recognised by Van Veen (1938).

Figure 11 shows correlations with the numerical model calculations M of the radar results E and F, and the ADCP results $\bar{R}$ and $\nabla\zeta$. These results are all essentially similar to those described from Figure 10, again illustrating the
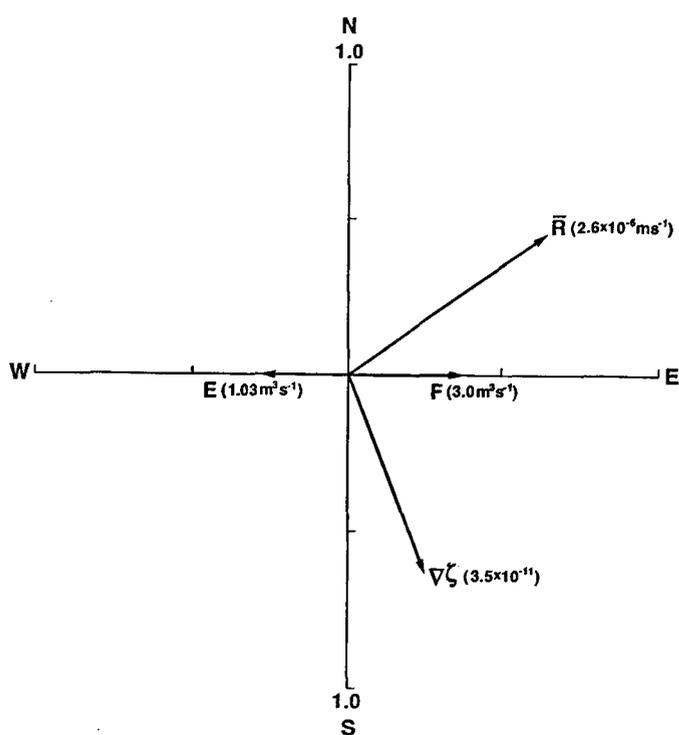
Figure 11

Complex correlations (r, θ) between M and E, F, R̄ and ∇ζ. Arrow lengths represent amplitude r and θ orientation for maximum M. For E, θ = 180° indicates negative correlation between the scalars E and M. Variances corresponding to M = 1 m³ s⁻¹ shown in brackets. M, E, F, R̄ and ∇ζ as defined in caption for Figure 10.

opposing nature of E and F. The figure also shows that M is a maximum when R̄ is aligned 35°N of east as anticipated from the Channel geometry.

This figure also emphasises that sea level gradients will be maximum across the Channel. Cartwright and Crease (1963) and Prandle (1978) estimated a mean cross-Channel sea level difference of 8 cm. For a width of 34 km and the relationship between R̄ and ∇ζ shown in Figure 9, this would correspond to a net residual flow of 67,000 m³ s⁻¹.

SUMMARY OF RESULTS

By combining results from five monthly H.F. radar deployments on the French coast with five on the English coast, surface currents across the full width of the Dover Strait have been measured. Simultaneous measurements of current profile at a single point in mid-Channel were made for a total of five months using a bottom-mounted ADCP. These measurements have been analysed to provide detailed descriptions of both tidal and residual flows.

Tidal current ellipse distributions are established and it is shown that the M_2 tidal flow through the strait generates a tidal residual drift of 36,000 cm³ s⁻¹.

The localised surface current response to wind forcing follows the classical Ekman theory with a veering of the order of 20° to the right of the wind and currents of the order of 1.6 % of the wind speed (at 10 m s⁻¹).

A modal analysis of the time-varying residual currents identified predominant modes corresponding to axial flows through the straits. Correlations of these corresponding modal time series with wind recordings provided a quantitative estimate of wind-forced fluxes through the Channel consistent with earlier modelling studies.

The time series associated with this predominant mode indicated occasional oscillations of periods between 20 to 30 hours with amplitudes an order of magnitude greater than the longer-term wind-driven fluxes. These data also indicated pronounced semi-diurnal oscillations associated with tide-surge interaction. However, there was no clear evidence of any significant seasonal component (other than that directly associated with wind forcing). Likewise, apart from the net tidal residual flow estimated at 36 x 10³ m³ s⁻¹ (Prandle et al., 1993 a) and a net wind driven flow estimated (Prandle et al., 1993 b) as 45 x 10³ m³ s⁻¹ the long term (remaining) Eulerian residual current through the straits was estimated as 6 x 10³ m³ s⁻¹, providing a net long-term residual flux of 87 x 10³ m³ s⁻¹ (the latter two residual components assume that the depth-averaged velocity is 0.75 of the surface residual - as calculated from ADCP measurements).

Analysis of five months of ADCP data involved the fitting of observed tidal current ellipse profiles to theoretical profiles. A similar model for residual current profiles yielded a value for the quadratic bed stress coefficient of 0.0025.

Using this model to fit observed ADCP data, it is shown that the measured residual currents and corresponding computed residual surface gradients are not generated by localised wind forcing. Their values are an order of magnitude greater than the latter and represent a response to a much wider-scale forcing.

The wind-driven residual transports computed from the radar measurements are in broad agreement with values from a numerical model simulation. However the radar results reveal opposing responses between the English and French sections, indicating counter-flows across the Strait not resolved by the model. Thus while the residual currents from the ADCP measurements are significantly correlated with aligned flows both calculated by the model and measured from the French radar sites, these currents are negatively correlated with corresponding flows from the English radar sites. Such opposing flows are shown in modelling studies of surge propagation where a large depression centred over the North Sea generates simultaneously flows eastwards in the Channel and southwards along the east coast of England.

Acknowledgements

POST SCRIPT

The results of this paper were presented for the first time at the Brest symposium in September 1992. In the same session, results of a modelling study by Salomon *et al.* were presented showing comparable residual flow calculations as follows:

	Radar measurements	Model[+] calculations
Tidal residual	36,000	37,400
Wind forcing	$0.83 \times 10^6 \tau \cos$ $(\phi+167°)$	$1.1 \times 10^6 \tau \cos$ $(\phi +174°)$
Net annual mean flow	87,000	90,500*
(* second half of 1990)	Units m^3 s^{-1} into the North Sea.	

The excellent agreement between these two sets of results indicates that close convergence has been achieved after over seventy years of research.

+ *Salomon* et al. *(this volume).*

REFERENCES

Cartwright D.E. and J. Crease (1963). A comparison of the geodetic reference levels of England and France by means of the sea surface. *Proc. R. Soc., Lond., A*, **273**, 558-580.

Flather R., R. Proctor and J. Wolf (1991). Oceanographic Forecast Models, in: *Computer Modelling in the Environmental Sciences*, D.G. Farmer and M.J. Rycroft, editors. Clarendon Press, Oxford, UK, 15-64.

Klinck J.M. (1985). EOF analysis of central Drake Passage currents from DRAKE 79. *J. phys. Oceanogr.*, **15**, 288-298.

Knight P.J., M.J. Howarth, D. Flatt and S.G. Loch (1992). Current profile and sea-bed pressure and temperature records May 1990-July 1991 Dover Strait. POL Report No. 22 (unpublished).

Oerlemans J. (1978). Some results of a numerical experiment concerning the wind-driven flow through the Straits of Dover. *Dt. hydrogr. Z.*, **31**, 182-189.

Pingree R.D. and K. Maddock (1977). Tidal residuals in the English Channel. *J. mar. biol. Ass. U.K.*, **58**, 965-973.

Pingree R.D. and D.K. Griffiths (1980). Currents driven by a steady uniform wind stress on the shelf seas around the British Isles. *Oceanologica Acta*, **3**, 2, 227-236.

Prandle D. (1975). Storm surges in the southern North Sea and River Thames. *Proc. R. Soc., Lond., A*, **344**, 509-539.

Prandle D. (1978). Residual flows and elevations in the southern North Sea. *Proc. R. Soc., Lond., A*, **359**, 189-228.

Prandle D. (1980). Co-tidal charts for the southern North Sea. *Dt. hydrogr. Z.*, **33**, 68-81.

Prandle D. (1982). The vertical structure of tidal currents and other oscillatory flows. *Continent. Shelf Res.*, **1**, 191-207.

Prandle D. (1984). A modelling study of the mixing of ^{137}Cs in the seas of the European continental shelf. *Phil. Trans. R. Soc., A*, **310**, 407-436.

Prandle D. (1987). The fine-structure of nearshore tidal and residual circulations revealed by H.F. radar surface current measurements. *J. phys. Oceanogr.*, **17**, 2, 231-245.

Prandle D. (1991). A new view on near-shore dynamics based on observations from H.F. radar. *Prog. Oceanogr.*, **27**, 403-438.

Prandle D. and J. Matthews (1990). The dynamics of nearshore surface currents generated by tides, wind and horizontal density gradients. *Continent. Shelf Res.*, **10**, 665-681.

Prandle D. and R. Player (1993). Residual currents through the Dover Strait measured by H.F. Radar. to appear in *Estuar. coast. Shelf Sci.*

Prandle D., S.G. Loch and R. Player (1993). Tidal flow through the Dover Straits. to appear in *J. phys. Oceanogr.*

Van Veen J. (1938). Water movements in the Straits of Dover. *J. Cons. int.Explor. Mer*, **14**, 2, 130-151.